journal homepage: www.intl.elsevierhealth.com/journals/cmpb

Anisotropic finite element modeling for patient-specific mandible

Sheng-Hui Liao, Ruo-Feng Tong, Jin-Xiang Dong*

State Key Laboratory of CAD and CG, Department of Computer Science and Engineering, Zhejiang University, Hangzhou, China

ARTICLE INFO

Article history:
Received 26 March 2007
Received in revised form
15 June 2007
Accepted 17 September 2007

Keywords:
Anisotropic material
Automatic mesh generator (AMG)
Complete mandible model
Patient-specific
Finite element method

ABSTRACT

This paper presents an ad hoc modular software tool to quasi-automatically generate patient-specific three-dimensional (3D) finite element (FE) model of the human mandible. The main task is taking into account the complex geometry of the individual mandible, as well as the inherent highly anisotropic material law. At first, by computed tomography data (CT), the individual geometry of the complete range of mandible was well reproduced, also the separation between cortical and cancellous bone. Then, taking advantage of the inherent shape nature as 'curve' long bone, the algorithm employed a pair of B-spline curves running along the entire upper and lower mandible borders as auxiliary baselines, whose directions are also compatible with that of the trajectory of maximum material stiffness throughout the cortical bone of the mandible. And under the guidance of this pair of auxiliary baselines, a sequence of B-spline surfaces were interpolated adaptively as curve cross-sections to cut the original geometry. Following, based on the produced curve contours and the corresponding curve cross-section surfaces, quite well structured FE volume meshes were constructed, as well as the inherent trajectory vector fields of the anisotropic material (orthotropic for cortical bone and transversely isotropic for cancellous bone). Finally, a sensitivity analysis comprising various 3D FE simulations was carried out to reveal the relevance of elastic anisotropy for the load carrying behavior of the mandible.

1. Introduction

An understanding of the biomechanics of the mandible is important for several reasons. It may give us an insight into the factors that determine mandibular bone structure. Being a numerical method for structure analysis suitable for the inhomogeneity, anisotropic material properties and complex boundary conditions of biological structures, FE analysis has become a popular analytical tool in biomechanical studies. Unfortunately, a major drawback of this method is the large amount of manual efforts required to generate high quality mesh model, especially for complex irregular structures such as the mandible.

Although the need for accurate FE models of the complete range of mandible in realistic simulation is now becoming more acknowledged, modeling of the complete mandible is not a trivial endeavor, due to their complex 3D geometry and boundary conditions, and the mixture of different load bearing parts and material properties. Therefore, most studies are limited to examination of exemplary and simplified models that often have to be build with intensive manual efforts which are very time consuming [1,2]. This way general statements

* *Corresponding author at*: P.O. Box 1166#, Yuquan Campus, Zhejiang University, Hangzhou 310027, China. Tel.: +86 571 87933346; fax: +86 571 87982571.
E-mail address: liaoshenhui@zju.edu.cn (S.-H. Liao).
0169-2607/$ – see front matter © 2007 Elsevier Ireland Ltd. All rights reserved.
doi:10.1016/j.cmpb.2007.09.009

or average conclusions can be derived. However, analysis of selected patients in order to optimize the individual therapeutic strategy is not possible. In other words, it would be useful to generate patient-specific or subject-specific FE models from individual source data, such as CT data, which provides an efficient and realistic means to in vivo capture of the complex geometry of human anatomy in the clinic.

To create patient-specific models, the adoption of an automatic or semi-automatic mesh generator (AMG) is a forced choice when the FE method is to be compatible with the pace of the clinical practice or when it should be used to perform the analysis on a large population.

2. Background

There are a large number of general purpose techniques for automatic mesh generation in the literature, such as algorithms employed for generation of tetrahedral elements: Octree [3], Delaunay [4], and Advancing front [5,6]; for generation of hexahedral elements: Grid based approach [7], Medial surface methods [8], Plastering [9], and Whisker Weaving [10]. The interested readers are referred to survey papers [11,12] for a good review.

Unfortunately, most of these available AMGs target engineering design and analysis applications, which expect the geometry to be defined with CAD tools, and therefore are not, in general, well suited to deal with irregular biological structures [13]. Anyway, this kind of indirect modeling method has been used extensively, usually to build exemplary and simplified models mentioned above, by using widely available commercial CAD tools, for example EDS/ Unigraphics (Plano, TX), Pro/Engineer (PTC Inc., New York), Maya (Alias-Wavefront Inc.), to create solid CAD models, and then exporting to various well-established mesh generators of commercial FE software [14], for example ANSYS (ANSYS Inc., Houston, PA), and Marc (MSC Software, Redwood City, CA), to build FE models. Some authors provided interface programs to these commercial software tools, and developed semi-automatic workflows to build patient-specific models [15,16].

This paper focuses mainly on particular solutions for constructing patient-specific 3D FE models for the purpose of biomechanical FEM simulations. To the best of the authors' knowledge, an automatic and well-established 3D-meshing algorithm for general anatomical structures is still far from available. However, recent advances in the field have made some interesting tools available.

One fully automatic approach allows the direct generation of voxel meshes (also known as Cartesian meshes) from the CT data [17,18]. While this method is widely used to investigate small volumes of trabecular bones as imagined by micro-CT scanners [19,20], its application to whole bones has been criticized, due to its inaccuracy in representing the geometry, and the large number of elements required to build the model [21].

Several authors tried to handle the problems of the voxel-based meshes. Camacho et al. [22] improved upon previous approaches by smoothing the irregular boundaries at model surfaces and material interfaces. Wang et al. [23] employed a tetrahedronization scheme that incorporates marching-cubes surface smoothing together with a smooth-distortion factor. Kaminsky et al. [24] developed an automated mesh-generator that combines the advantages of voxel-based generation with improved representation of the geometry by displacement of nodes on the object-surface. However, these methods still have the inherent problem of resulting in a large number of elements.

On the other hand, due to its rigorous adaptability to structures with geometric complexities, tetrahedral meshes are always quite popular and generated from medical images by various methods in the last few years. Lin et al. [25] generated a tetrahedral FE mesh for the maxillary second premolar based on moving nodes of uniform cube approach. Gao et al. [26] proposed an interactive division scheme to generate 3D tetrahedral elements for complicated, multi-connected biomedical structures, such as a tooth-mandible structure. Archip et al. [27] constructed anatomical models from medical images by 3D Delaunay tetrahedralization using a distance map and bit volume structures. Kwon et al. [28] built triangulated surfaces from contours on medical images, and then generated tetrahedral mesh by an Advancing front algorithm. Erdmann et al. [29] also employed an Advancing front algorithm to generate volumetric tetrahedral meshes for human mandible from non-manifold surface grids after successive grid coarsening, smoothing, and interactive grid editing.

Because a good mesh of hexahedral elements can vastly reduce the number of elements and often perform better than tetrahedral mesh in the analysis stage, several authors tried to develop unstructured hexahedral from medical images. Viceconti et al. [31,32] extensively studied an unstructured hexahedral grid generator by means of a generalized grid projection algorithm called Hexar [30], which was found to provide enough automation, intrinsic accuracy, robustness and generality to be used in clinical applications. While, in order to achieve a well-conditioned mesh, the models usually required a mesh refinement which increased the models' size. Kober et al. [33] provided a case study of the human mandible for the applicability of a combinatorial approach for the generation of hexahedral meshes by means of successive dual cycle elimination. The input surface triangulation required a substantial mesh reduction and a suitable conversion into a quadrilateral surface mesh. And the resulting combinatorial meshes needed gradient-based optimized smoothing with mesh untangling techniques to yield embeddings of satisfactory quality. Shim et al. [34] used sparse CT datasets to generate hexahedral models of the femur and pelvis, employing high order cubic Hermite basis functions and least-square to fit the mesh to the dataset. Relatively high peak errors occur in some regions of the pelvis, and the peak errors get worse as the mesh becomes coarser. Zhang et al. [35,36] employed a top-down octree subdivision coupled with an extended dual contouring method to rapidly extract adaptive tetrahedral and hexahedral meshes from volumetric imaging data.

Another kind of interesting methods to build patient-specific FE models is template-based approach. Couteau et al. [37] described an algorithm called mesh-matching to transform a structured mesh of femur, manually created by an expert operator, to the same type of bone. Baghdadi et al. [38] presented a similar method, with a tetrahedral mesh, instead of hexahedral mesh, as the baseline EF model. Both of these approaches tend to generate poor quality (even distorted)

elements at the boundaries, which need mesh smoothing and/or mesh untangling techniques to yield satisfactory quality embeddings.

3. Design considerations

It should be noted that, being a numerical modeling method, the validity of the FEM results is mainly dependent upon three types of modeling factor [26]. The first factor is the similarity of the FE model to the real structure of the object to be analyzed. Excessive simplifications in geometry will inevitably result in considerable inaccuracy in the analysis. The second factor is associated with the modeling of the material properties of the structure studied. Setting of material parameters improperly will lead to erroneous results. The third factor is the effectiveness of modeling the boundary conditions, i.e. the force loading and displacement boundary conditions.

Among the above three factors that determine the validity of FEM results, the boundary conditions can be modified interactively. By applying a new set of boundary conditions and re-executing the FEM software, one can readily get a new set of simulation results. This is especially easy nowadays since the computer hardware is so powerful in terms of speed and memory.

The geometric modeling, however, is a rather difficult task when AMGs are not available. Although the available tools have significantly improved over the last few years, the generation of the mesh remains a critical activity in most studies based on the FEM. This particularly holds true in biomedical applications where the shape of the object to be meshed is usually quite complex. In addition, we have noticed that the base geometry information to build the FE model is extracted directly on parallel image slices, e.g., parallel contours or grid points, in most of previous biomedical FE modeling approaches [17–28,34–36]. This tends to generate poor quality elements at the boundaries. And the final mesh structure aligns inherently with the parallel image slices, which does not properly account for the preferential orientation feature of the biomedical organs.

The assignment of proper material properties to the FE model is also a fundamental step to ensure predictive accuracy. The modeling of biological tissues, such as bone related organs, is a very difficult task because of their inherent inhomogeneous and anisotropic character [39]. The inhomogeneous character is in some sense “directly” accessible via the CT data based on the relationship between CT numbers, Hounsfield Unit (HU), and bone material properties [40–42].

Unfortunately, this is not the case for the trajectories of anisotropic elasticity. To address this problem, many researchers investigated the anisotropic material property of bone tissues by various experimental methods.

Currently available human mandible material property measurements are almost concerning the cortical bone, such as the studies of Ashman et al. [43], Lettry et al. [44] Nomura et al. [45], Schwartz-Dabney and Dechow [46,47]. It is commonly accepted that the direction of maximum stiffness is primarily oriented longitudinally in the diaphysis of the curve long bone, and the elastic modulus is greatest in that direction compared to radial and tangential (circumferential) orientations.

While, there still lacks of enough experimental measurements for mandibular cancellous bone. The only experimental anisotropic study of cancellous bone for human mandible we could find is presented by O’Mahony et al. [48], which suggested a model of transverse isotropy for cancellous bone in the jaw, where the symmetry axis is along the infero-superior (weakest) direction.

So, without an automatic and well-defined assignment scheme, it is impossible to generate the principal orthotropic material orientations (orientation of the principal symmetry axes of orthotropy), which change from point to point in the complete mandible. And most work done in the biomechanics field adopted oversimplified isotropic material law due to its simplicity, which in fact should use orthotropic symmetry for bone tissues. Several authors tried to incorporate orthotropic (or simplified transversely isotropic) elasticity into their FE models, but limited to only a segment of the mandible, whose longitudinal axis is almost on a common direction [49–51].

Motivated by these evidences and considerations, we developed a new modular software tool in the self-developed surgical assisted system *Universal Surgical Integration System* (USIS), to build high quality patient-specific 3D FE model of the human mandible from CT data. The long-term goal of this research is to provide a complete solution for constructing anisotropic FE model for the purpose of biomechanical FEM simulations in the clinic.

The basic thought is to take advantage of the fact that the direction of maximum stiffness of cortical bone is primarily oriented longitudinally in the diaphysis of the long bone, although it is an irregular ‘curve’ long bone for the mandible—which is the very difficult problem discouraged previous studies in this area. In other words, both meshing and anisotropic material assignment could be considered together in the biomechanical modeling.

The solution is first to construct a pair of B-spline curves capturing the inherent shape of the mandible as auxiliary baselines. Then interpolate a sequence of B-spline surfaces, under the guidance of this pair of auxiliary baselines, as curve cross-sections to cut the original geometry. Following, the resulting curve contours are well processed to build the volumetric mesh, whose structure properly accounts for the preferential directions dictated by the anisotropic material characteristics. Finally, a well-established orthotropic principal axes orientation assignment scheme is used to establish the final anisotropic FE model.

The detailed modeling procedure is described in Section 4. Then a sensitivity analysis is carried out in Section 5 to reveal the relevance of elastic anisotropy for FEM simulations. And in Sections 6 and 7, we will draw some conclusions and discuss further work.

4. System description

4.1. *Pre-processing of original CT data*

The starting point of our investigation was a well-reproduced individual geometry of the complete range of mandible, including the separation between cortical (compact) and cancellous bone, such as Fig. 1 illustrates. This data basis origi-

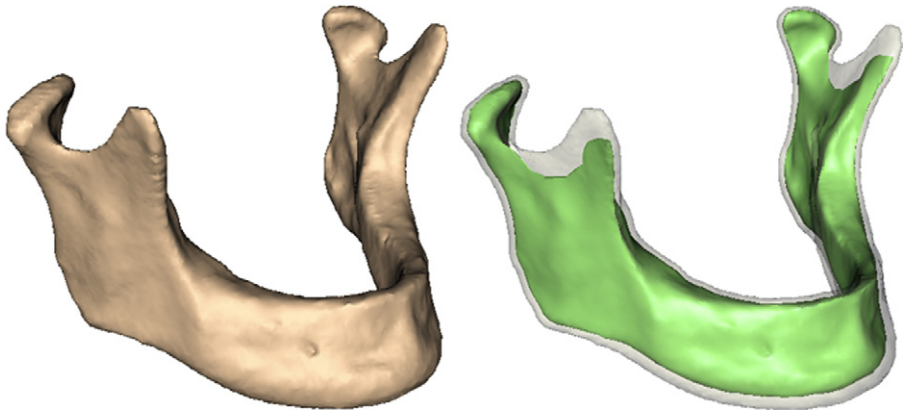

Fig. 1 – Individual geometry of the complete range of mandible.

nally stemmed from CT data, which was processed by another 3D segmentation modular software tool in the USIS system. And the iso-surfaces were extracted by the Discretizied Marching Cube algorithm [52], in a 'tiled surface' form.

The tiled surface contained numerous poorly shaped triangles, and was too large by several orders of magnitude to create FE model directly. Erdmann et al. [29] employed successive grid coarsening, smoothing, and interactive grid editing to improve the base surface of a mandible, which was input directly to an Advancing front algorithm to generate tetrahedral meshes. However, this method required lots of manual interactive editing, and was not convenient for local mesh density control.

To avoid these problems, some ad hoc post-processing was investigated to re-mesh the tiled surface, as well as build the anisotropic FE model, as described in the following subsections.

4.2. *Extract crucial geometry by curve cross-section surfaces*

As mentioned before, to integrate the anisotropic material characteristics (mainly the material orientation) assignment scheme into the FE mesh generator, the algorithm needs to take advantage of the fact that the direction of maximum stiffness of cortical bone is primarily oriented longitudinally in the diaphysis of irregular 'curve' long bone. One possible choice is making use of the center medial axis line of the mandible as auxiliary baseline to approximate that direction. While, it is a too coarse capture of the mandibular geometry, especially for the posterior regions, like condylar process and ramus.

Instead, the algorithm employed a pair of B-spline curves running along the entire upper and lower mandible borders as auxiliary baselines, such as Fig. 2(a) shows, which were established by interpolating several offsetting points on the mandible borders via an interactive graphical user interface (GUI). Obviously, this pair of auxiliary baselines had a much better capture of the inherent shape of the mandible than the center medial axis line. In addition, they provided a convenient reference framework to generate cross-section surfaces to re-mesh the original tiled surface. This was implemented by allocating a pair of movable sliding points on the auxiliary baselines, such as the pair of small red balls on the baselines in Fig. 2(b)–(d). And a sequence of this pair of sliding points' locations determined the initial positions of the cross-section surfaces.

To aid in the exposition, we first describe how one curve cross-section surface was established, as demonstrated in Fig. 2(b) and (c). Once the locations of this pair of sliding points were chosen, their mean tangential (longitudinal) direction on the auxiliary baselines was used to determine a base direction plane, such as the green plane depicted in the figure. And a center B-spline curve linking the pair of sliding points as fixed end points was generated, with one or more control points, which were movable freely in the base direction plane, to control the curvature of the curve, such as the yellow B-spline curve and the white control ball on it shown in the figure. Then the curve cross-section surface was established by sweeping the curvature control B-spline curve in the direction perpendicular to the base direction plane, such as the red B-spline surface depicted in the figure.

Of course, the users did not need to generate all of the cross-section surfaces one by one manually. What needed to do was just constructing several critical cross-section surfaces on the mandible. For example five surfaces were employed, as demonstrated in Fig. 2(d): one cross-section surface was put at the position of center sagittal plane, two symmetry surfaces were located at the left and right mandibular angles, and another two were positioned at the left and right mandibular notches (bifurcation regions). These surfaces were initially laid nearly perpendicular to the borders of the mandible, and their curvatures were then properly adjusted to account for the preferential direction dictated by the configuration of the mandible, as well as the material orientation. More precisely, these cross-section surfaces were tuned to be perpendicular, as possibly could, to the direction of maximum stiffness at the corresponding local regions according to those experimental measurements.

Had these critical surfaces fixed, the in-between curve cross-section surfaces were generated automatically by interpolating the locations of the sliding points on the auxiliary baselines as well as the curvature of the center control B-spline curve. The number of the interpolated cross-section surfaces was determined by several factors discussed in the following subsection, unless the user specified a count value.

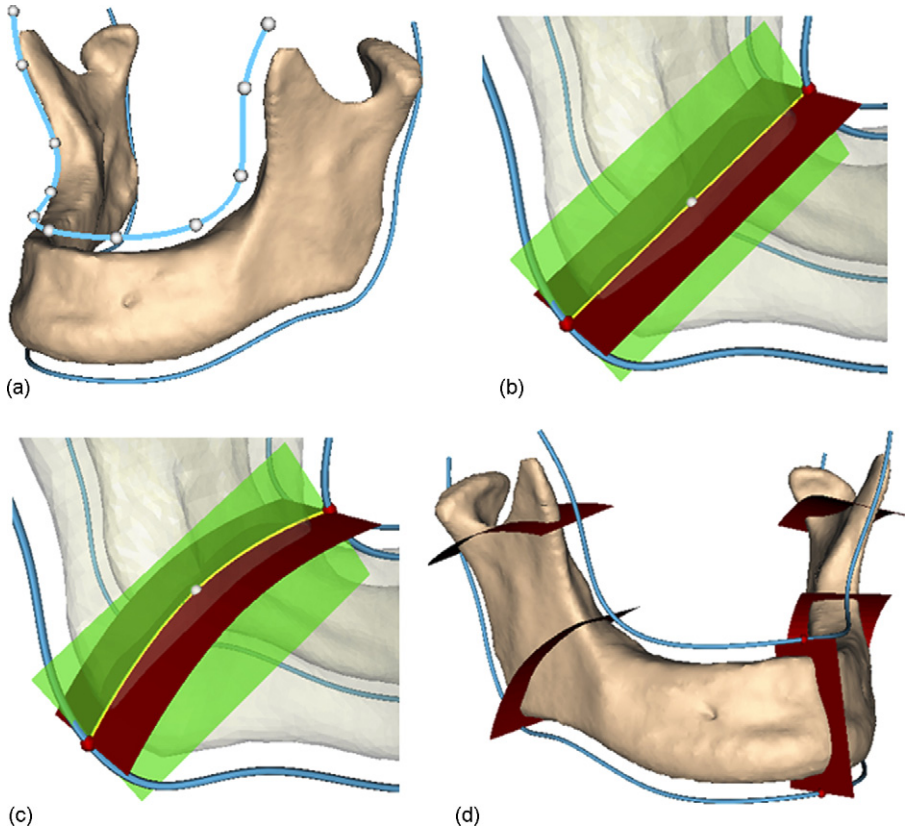

Fig. 2 – Construction of auxiliary baselines (a) and curve cross-section surfaces; (b–c) illustrate the procedure to establish one curve cross-section surface; (d) demonstrates the locations of several critical cross-section surfaces on the mandible.

Once these curve cross-section surfaces were constructed, they were used to intersect with the original tiled surface models. Each intersection produced one or more closed multi-segment curves which were least-square fitted with Non Uniform Rational B-spline (NURBS), such as the purple contours shown in Fig. 3. These NURBS contours not only ensured that the original crucial geometry of the mandible was kept, but also provided a continuous tangential direction, which would be employed latter to interpolate the orthotropic circumferential material orientation. Remember that there were two layers of tiled surface, the algorithm recorded that information by a flag to distinguish the out layer NURBS contours and the internal layer NURBS contours.

4.3. *Generate complete mandible volume mesh*

For now, assume that the algorithm was given a sequence of curve cross-section surfaces as well as the corresponding NURBS contours. To construct the volume mesh, the NURBS contours needed to be subdivided into discrete contours with geometrical key points first.

These key points were distributed adaptively instead of equidistantly along the contours. In fact, the adaptive distribution of the key points as well as the optimal interpolation of cross-section surfaces in the previous subsection accommodated the users a full control of the mesh density. In particular, the algorithm changed the mesh density in several ways:

1. Locally in neighborhood of biomechanics significant regions, such as the condyles and the force loading area.
2. In the relatively thin surrounding component, such as the cortical bone of the alveolar ridge. This could be detected quickly by the distance between the out layer contours and the corresponding internal layer contours.
3. With respect to the curvatures, including the curvature of the auxiliary baselines as well as the surface curvature of the original model. Higher curvature required finer meshes.

In addition, these generated key points were given a regular and consecutive numbering to identify their 3D location, including which cross-section surface belonging to, and whether stemmed from out layer contours or internal layer contours. The result was that all geometric features could be pinpointed and processed directly and a full controlled handling is possible.

The remaining outline was now to construct the FE mesh by a two-step automatic workflow.

The first step was to build the volumetric mesh for the cortical bone of the mandible (the region enclosed by both the original out and internal surface) from the above-generated key points, by a modified Boundary Constrained Delaunay Triangulation procedure, with these contour segments between key points reserved. And the algorithm also employed a simple centroid point insertion strategy, if necessary, to ensure the quality of the produced tetrahedron element. The newly inser-

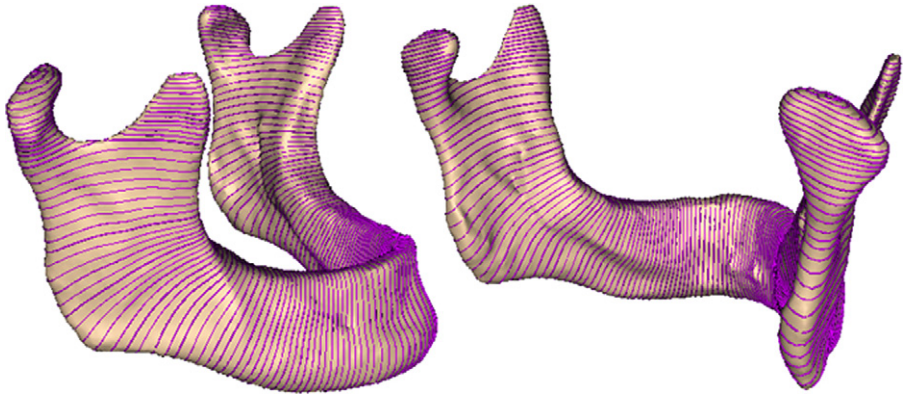

Fig. 3 – Distribution of NURBS contours on the mandible.

tion points were also given a regular numbering to identify which interval zone (segmented by the cross-section surfaces) belonging to.

Having built the out layer mesh for the cortical bone, the second step was to construct the interior volumetric mesh for the cancellous bone. This was solved by an advancing front algorithm, with the initial active front detected by the key points numbering identified belonging to the internal layer contours.

An example of resulting volumetric mesh for the mandible was given in Fig. 4. We can see that quite well structured FE mesh was created, whose structure properly accounted for the preferential direction dictated by the configuration of the mandible as well as the anisotropic material characteristics. The element shape quality measure, using the mean-ratio metric [53] (the range of valid values varies from 0 to 1, attaining 1 for the ideal element shape), demonstrated that the resulting mesh usually had an overall average value of more than 0.82. Few poorly shaped elements might exist in the interior of the mesh, with the minimum value closed to 0.45, because the Advancing front algorithm was employed for the cancellous layer.

In addition, the FE mesh captured the shape of original mandible model very well, such as shown in Fig. 5, and preserved as much of the intrinsic qualities of the original model as possible, which demonstrated the accuracy of the methodology.

4.4. *Estimate trajectories of anisotropic elasticity*

We shall now describe how to build the final anisotropic FE model with a well-established anisotropic material characteristics assignment scheme. As discussed previously in Section 3, the main difficult problem is to figure out the principal orthotropic material orientations of the cortical bone, which change from point to point in the complete mandible.

4.4.1. *Principal orthotropic material orientations for cortical bone*

Based on those experimental measurements that Schwartz-Dabney and Dechow provided [43–47], the algorithm constructed radial, tangential (circumferential), and axial (longitudinal) trajectories to define the principal orthotropic material orientations at each location within the cortical bone of the mandible. In other words, three perpendicular vector fields needed to be calculated.

While, in practical discrete implementation, the algorithm just needed to determine the spatial angles of the axes of orthotropy at each nodes of the FE mesh. And fortunately, the way our methodology building the volumetric mesh pro-

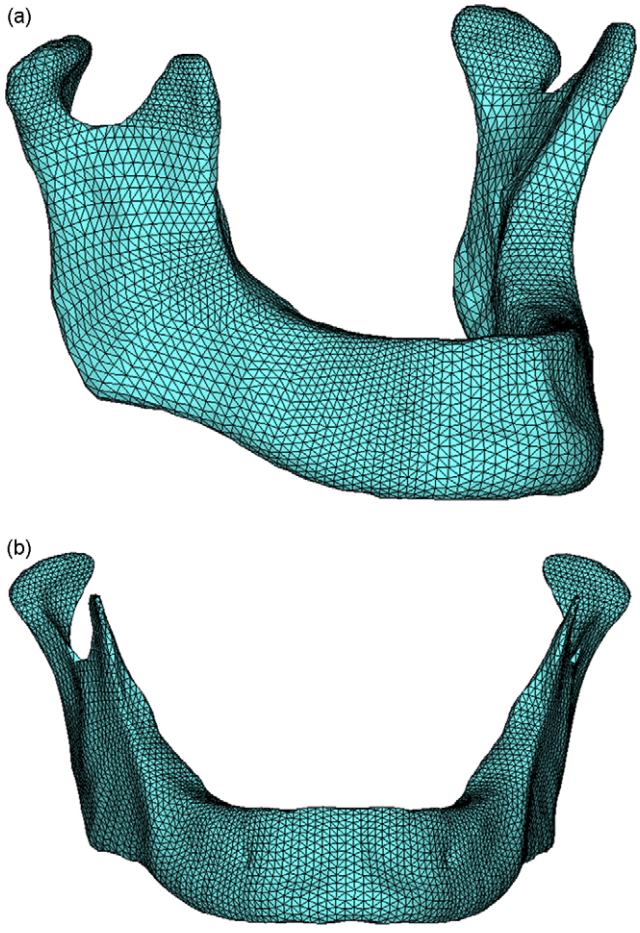

Fig. 4 – Resulting volumetric meshes for the mandible; (a) illustrates the boundary mesh of the cortical bone, and (b) is the cancellous bone.

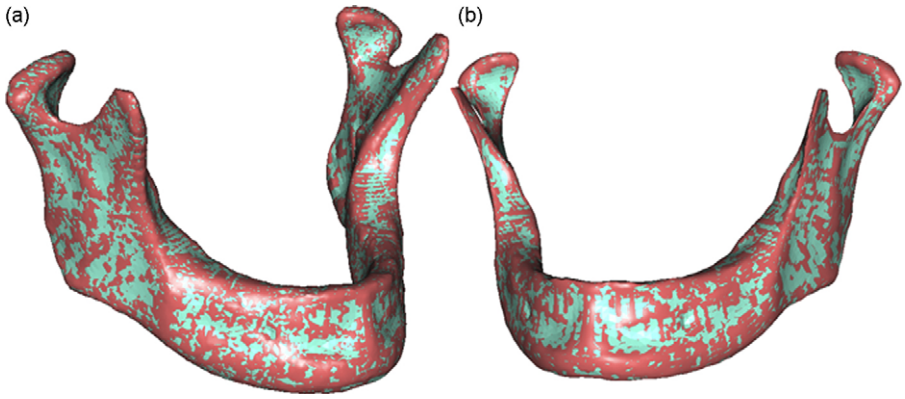

Fig. 5 – Original geometry model (red color) and overlaying boundary mesh of FE model (blue color); (a) illustrates for the cortical bone, and (b) for the cancellous bone.

vided a convenient base on which to estimate these spatial directions.

Remember that there were two kinds of finite element nodes in the cortical volumetric mesh: those subdivision key points on the NURBS contours, and those newly insertion centroid points during the Delaunay Triangulation procedure. This implied that the algorithm could first calculate the orthotropic material orientations of the regular key points, then from which derive that of the insertion points.

Because the key point nodes located directly on the out and internal surface mesh of the cortical layer, it was convenient to use their surface normal directions as the radial material orientation, such as these red vectors depicted in Fig. 6(a).

With regard to the tangential (circumferential) material orientation, it should be remembered that those cross-section surfaces were initially laid nearly perpendicular to the borders of the mandible, and then tuned to be perpendicular, as possibly could, to the direction of maximum stiffness at the corresponding local regions according to those experimental measurements. And the contour segments between key points were reserved in the Delaunay Triangulation. So, it was reasonable to use the tangential direction on the NURBS contours to represent the tangential (circumferential) material orientation of these key point nodes, such as these green vectors depicted in Fig. 6(b). In addition, the regular, systematic numbering of the points in the previous subsection provided a direct and pinpoint access to the corresponding location on the NURBS contours.

Finally, the axial (longitudinal) material orientation, that was the direction of maximum stiffness, could be derived from the cross product of the radial and tangential (circumferential) material orientations, such as these blue vectors depicted in Fig. 6(c).

For the purpose of computing the material orientations of these insertion points, the algorithm employed a weighted interpolation scheme. It also took advantage of the regular, systematic numbering of the points that recorded which interval zone (segmented by two nearest cross-section surfaces) the insertion point belonging to. And through experiments, we found that a two-step projections scheme worked in a robust way.

First, projected the insertion point onto the two nearest cross-section surfaces separately, and recorded the distances to the projection points as Dp_1 and Dp_2. Following, for these surface projection points, calculated the nearest points on the corresponding out layer NURBS contours and internal layer NURBS contours, if exist, and recorded these distances as Doc_i for out contours and Dic_i for internal contours, where $i=1$ and 2 for the first and second cross-section surface, respectively. Then estimated the radial or tangential (circumferential) material orientations at these nearest points on the NURBS contours like those key points, and recorded as Voc_i for out contours and Vic_i for internal contours. Then, the following interpolation formula, with the inverse distance proportions as weights, was employed to calculate the radial or tangential (circumferential) material orientation of the insertion point:$V = \sum_{i=1,2}(\mathrm{Voc}_i \cdot \mathrm{Woc}_i + \mathrm{Vic}_i \cdot \mathrm{Wic}_i) \cdot Wp_i$, where $Wp_1 = Dp_2/(Dp_1 + Dp_2)$, $Wp_2 = Dp_1/(Dp_1 + Dp_2)$, and $\mathrm{Woc}_1 = \mathrm{Dic}_1/(\mathrm{Dic}_1 + \mathrm{Doc}_1)$, $\mathrm{Wic}_1 = \mathrm{Doc}_1/(\mathrm{Dic}_1 + \mathrm{Doc}_1)$, $i=1$ and 2. At last, the axial (longitudinal) material orientation of the insertion point was derived from the cross product of the radial and tangential (circumferential) material orientations.

Although this two-step projections scheme seemed a little complicated compare to other simpler interpolation method, it ensured the quality of the material orientations of these insertion points. In addition, there were only a small number of insertion points produced in our mesh generation methodology (usually less than 200).

An example of resulting principal orthotropic material orientations of the mandibular cortical bone was given in Fig. 6, presented in vectorial form at the nodes of FE mesh (a–e) and the centers of tetrahedral (f).

4.4.2. *Transversely isotropic material orientations for cancellous bone*

As discussed previously in Section 3, there still lacks of enough experimental measurements for mandibular cancellous bone. The only experimental anisotropic study of cancellous bone for human mandible we could find is presented by O'Mahony et al. [48], which suggested a model of transverse isotropy for cancellous bone in the jaw, where the symmetry axis is along the infero-superior (weakest) direction.

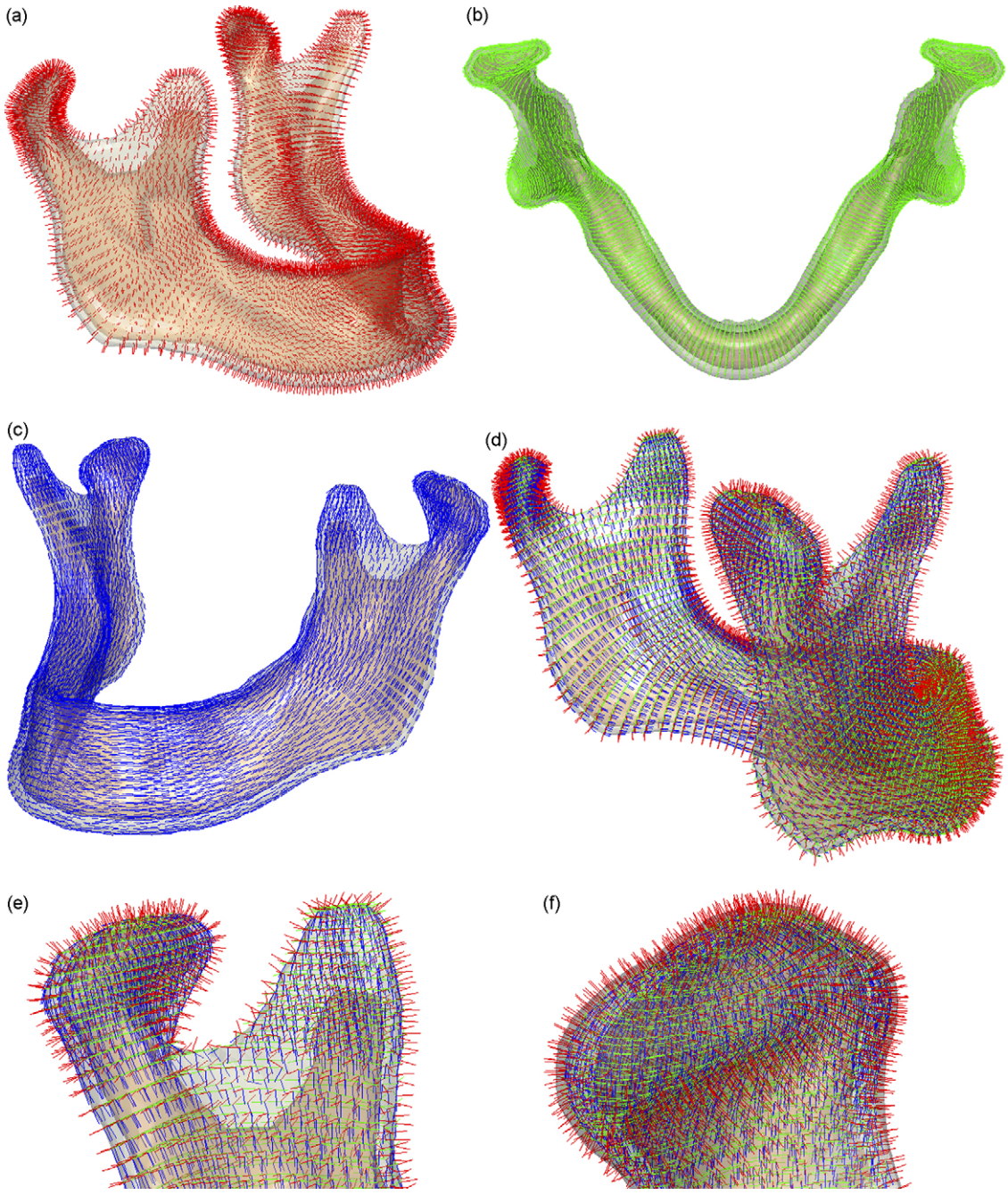

Fig. 6 – Principal orthotropic material orientations of the mandibular cortical bone presented in vectorial form: the radial, tangential (circumferential), and axial (longitudinal) directions are depicted by red, green and blue vector fields separately; (a–e) demonstrate at the nodes of FE mesh and (f) at the centers of tetrahedral inside the cortical bone.

Then, it was relative easy to define a local coordinate system, with one axis representing infero-superior direction of the mandible, for the whole cancellous layer.

It should also be pointed out that many researchers thought that, although lacks of experimental supports, the mandibular trabecular orientations are similar to patterns of the direction of maximum stiffness found in the overlying cortical bone [47,49]. If this hypothesis is true, our methodology should still work, if necessary, making use of the center middle axis line of the mandible as the third auxiliary baseline.

4.4.3. *Anisotropic material characteristics for FE model*

The remaining outline was now to assign the whole anisotropic material characteristics to the finite elements in the model, including the orientations of material axes and the elastic material properties.

For the purpose of computing the orientations of material axes of the finite elements of cortical layer, the algorithm employed an average interpolation procedure transferring the data of the FE nodes to the center of each FE tetrahedron, such as depicted in Fig. 6(f). And that of the cancellous finite ele-

Table 1 – Elastic coefficients for cortical (Cort.) and cancellous (Can.) bone of human mandible[a]

	E_1	E_2	E_3	G_{12}	G_{13}	G_{23}	ν_{12}	ν_{13}	ν_{23}
Cort.[b]	12.5	17.9	26.6	4.5	5.3	7.1	0.18	0.31	0.28
Can.[c]	0.21	1.148	1.148	0.068	0.068	0.434	0.055	0.055	0.322

[a] E_i represents Young's modulus (GPa); G_{ij} represents shear modulus (GPa); ν_{ij} represents Poisson's ratio.
[b] Elastic coefficients for cortical bone are based on [46,47]. The one-direction is radial, the two-direction is tangential (circumferential), and the three-direction is axial (longitudinal).
[c] Elastic coefficients for cancellous bone are based on [48,50]. The one-direction is infero-superior (the axis of transverse isotropy symmetry with the smallest of Young's modulus value), the two-direction is medial–lateral, and the three-direction is anterior–posterior.

ments just needed to use the same material axes of the whole cancellous layer.

With regard to the elastic material properties, since we focused on the impact of the tissue anisotropy on the simulation results rather than on the impact of the inhomogeneity, we kept the orthotropic elastic components constant over the mandible, differentiating only between cortical and cancellous bone, see Table 1. In addition, although the inhomogeneous character is in some sense "directly" accessible via the CT data based on the relationship between CT numbers, Hounsfield Unit (HU), and bone material properties [40–42] as discussed in Section 3, Lettry et al. [44] found there is only a weak correlation between the modulus values and the CT number of the mandible, and suggested that it would not be sufficient for accurate predictions of the bone properties from CT scans.

4.5. *Programming environment and hardware*

All these techniques have been implemented by Visual C++ 2005 (Microsoft Inc., Seattle, USA) as a modular software tool in the USIS system, running on a common Pentium IV personal computer.

5. Status report

5.1. *Simulation example and sensitivity analysis*

Finally, we provided an example and performed a group of FE simulations to investigate the effects of material anisotropy on the load carrying behavior of the human mandible.

As a first step in this direction, we integrated a simple titanium implant (4 mm diameter × 15 mm length, $E = 103.4$ GPa, $\nu = 0.35$) in the first molar region on the right hand side, and selected a simple load case: a static lateral bite on the implant based on biomechanical experiment. The boundary conditions, which were set interactively via the GUI system, were shown in Fig. 7(a), involving two kinds of masticatory muscles force (500 N), constraint on all three degrees of freedom for the front part of condylar process, and constraint on the freedom of bite direction for the top area of implant.

Numerical FE analysis function has not been included into the USIS system up to now. Instead an interface procedure was integrated to convert automatically the whole FE model into the FE software system ANSYS 9.0 (ANSYS Inc., Houston, PA, USA) for numerical simulations, by an APDL (ANSYS Parameter Design Language) script. In addition, all of the linear tetrahe-

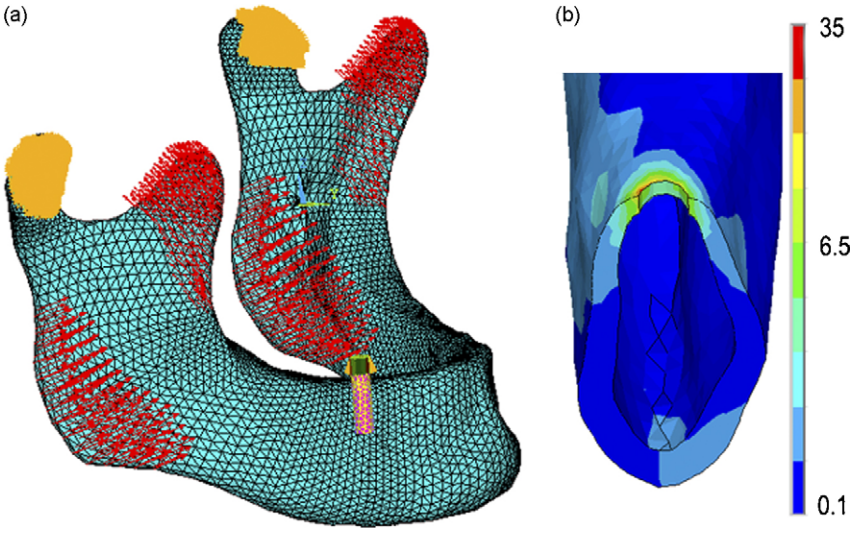

Fig. 7 – (a) Boundary conditions of the lateral bite loading simulation; (b) Von Mises stress distribution of the cortical bone for the fully anisotropic case.

Table 2 – Index of anisotropy according to Mülller-Hannemann et al. [49]

	$\alpha = 0$, isotropic	$0 < \alpha < 1$[a], increasing anisotropy	$\alpha = 1$, anisotropy	$1 < \alpha < 2$[b], decreasing anisotropy	$\alpha = 2$, isotropic
$E_1(\alpha)$	E_1	E_1	E_1	$E_1 + (\alpha - 1)(E_3 - E_1)$	E_3
$E_2(\alpha)$	E_1	$E_1 + \alpha(E_2 - E_1)$	E_2	$E_2 + (\alpha - 1)(E_3 - E_2)$	E_3
$E_3(\alpha)$	E_1	$E_1 + \alpha(E_3 - E_1)$	E_3	E_3	E_3
$\nu_{ij}(\alpha)$	ν_S	$\nu_S + \alpha(\nu_{ij} - \nu_S)$	ν_{ij}	$\nu_{ij} + (\alpha - 1)(\nu_h - \nu_{ij})$	ν_h
$G_{12}(\alpha)$	G_S	$G_S + \alpha(G_{12} - G_S)$	G_{12}	$G_{12} + (\alpha - 1)(G_h - G_{12})$	G_h
$G_{13}(\alpha)$	G_S	$G_S + \alpha(G_{13} - G_S)$	G_{13}	$G_{13} + (\alpha - 1)(G_h - G_{13})$	G_h
$G_{23}(\alpha)$	G_S	$G_S + \alpha(G_{23} - G_S)$	G_{23}	$G_{23} + (\alpha - 1)(G_h - G_{23})$	G_h

[a] $\nu_S = \max(\nu_{ij})$ and $G_S = (E_1/2)(1 + \nu_S)$.
[b] $\nu_h = \min(\nu_{ij})$ and $G_h = (E_3/2)(1 + \nu_h)$. $1 \le i, j \le 3$.

dral elements (4 nodes) were converted to parabolic elements (10 nodes), to ensure the numerical accuracy.

For the sensitivity analysis, as in Mülller-Hannemann et al. [49], we introduced an index of anisotropy α varying from isotropic material with a low Young modulus over fully anisotropic behavior again to isotropic material but with a high Young modulus, see Table 2. The cases with $\alpha = 0$, 0.25, 0.5, 0.75, 1.0, 1.25, 1.5, 1.75 and 2.0 were evaluated.

A detailed discussion of the FE simulations goes beyond the scope of this paper. We selected the displacement, Von Mises stress and Von Mises strain, which are widely referenced in FE studies, surrounding the bite region of mandible for the cortical bone and cancellous bone separately. Fig. 8 illustrated the peak values of these post-processing data items. And Fig. 7(b) displayed the Von Mises stress distribution of cortical bone for the fully anisotropic case ($\alpha = 1.0$).

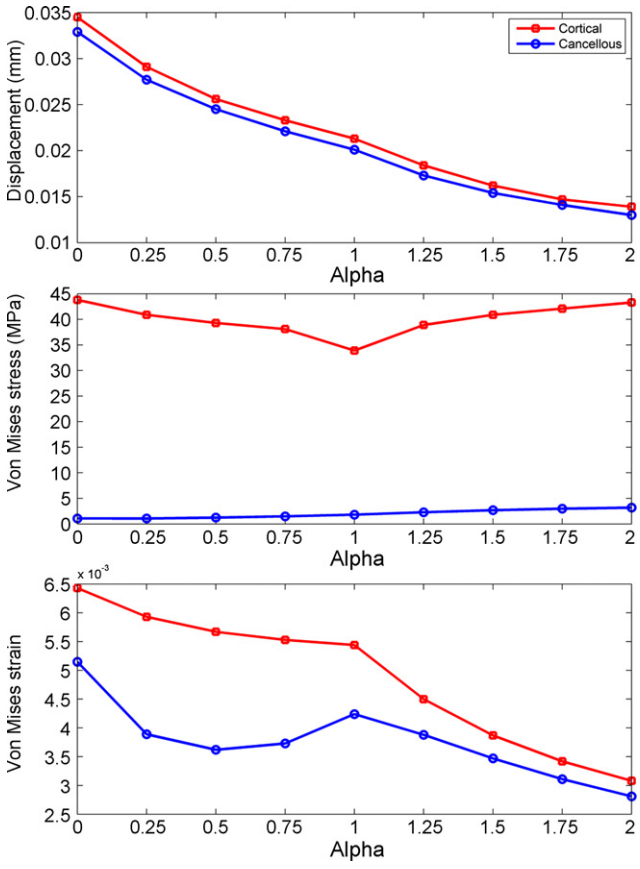

Fig. 8 – Peak values of post-processing simulation results for the displacement, Von Mises stress and Von Mises strain.

By elevating the index of anisotropy α, the algorithm was stepwise 'hardening' the mandible. Spontaneously, one would expect monotonous responses for those data items. This was true for the displacements and Von Mises strains. But for the Von Mises stresses of cortical bone, there was a minimum for the fully anisotropic case, such as Fig. 8 illustrated, indicating that this case was the most efficient configuration to reduce the intensity of stress and can withstand relatively large bite forces. Because of the significance of stress in bone remodeling and adaptation, this fact underlined the necessity of anisotropic simulation for the human mandible.

5.2. *Methodology strengths and limitations*

To the best of the authors' knowledge, there is no published study that develops an AMG technique integrated with anisotropic material characteristics assignment function in the biomedicine and biomechanics fields.

The orthotropic material property assignment to femur, not integrated in the AMG, has been adopted in recent studies. Liang et al [54] used only one local Cartesian coordinate system of femur with directions: medial–lateral, anterior–posterior, and superior–inferior, for the whole femur. Obviously, this method is oversimplified. Wirtz et al [55] cut the cadaveric femurs in 2 mm slices, which were scanned into a computer-based image processing system. On these images, the principal directions of stiffness of cancellous and cortical bone were determined manually using the orientation of the trabecular structures and the Haversian system. However, this method not only requires a lot of time and manual effort but it is also an error prone procedure. In addition, the complexity of the femur topology is much moderate as compared with the complete mandible structure involved in this paper.

To address this problem in mandible related biomechanics studies, we have developed an ad hoc modular software tool, which integrates an automatic anisotropic material characteristics assignment scheme into the FE mesh generator, to construct high quality patient-specific 3D FE models of the mandible.

In terms of geometry similarity, the mesh boundary captures the shape of original model very well, which demonstrates the accuracy of the methodology.

In terms of automation, the modular tool pays particular attention and allows a large degree of automation and is,

therefore, a quasi-standardized tool to generate anisotropic mandible models. The main manual work involves interactive creating of the pair of auxiliary baselines, and distributing several critical cross-section surfaces on the mandible, which can be done within a few minutes via the GUI system. And if it is necessary, we could promote the automatic level of these steps by making use of heuristic anatomical knowledge about the mandible, which is one of the main advantages of developing an ad hoc mesh generator.

In terms of efficiency, the relative computationally expensive phase is the extraction and subdivision of NURBS contours from the original model, usually costs 10–20 min on a common personal computer, which is in an acceptable period and compatible with the pace of clinical practice.

The initial sensitivity analysis reveals that the fully anisotropic (and so the most realistic) case achieves some kind of optimality in the sense of minimization of stress, which underlines the relevance of our anisotropic material characteristics assignment scheme.

We also acknowledge the limitations of our study. Firstly the underlying kinematical boundary conditions are simplified assuming loading conditions of only two kinds of acting forces. Hence, the incorporation of the mechanical influence of other muscles, ligaments, temporomandibular joint (TMJ), and so on, are necessary to obtain a numerical simulation more close to the in vivo conditions. However, this job mainly involves figuring out the nature of the forces and moments that act on the mandible during functioning, and setting up these conditions in the software tool is relative easy. Secondly is the generality, our method is specially designed for mandible. This is for the sake of making use at the fullest extent of the characteristic of some known bone (mandible), which is most frequently required in clinical settings. Moreover, it should be easily expanded to other 'long' bones, which can utilize the core spirits of our methodology.

6. Lessons learned

Information on the orientation of material axes is especially important for studies of regional differences and to approach questions relating bone function of bone adaptation and growth.

Taking advantage of the inherent shape nature as 'curve' long bone and anisotropic material orientation characteristics of the mandible, the algorithm employs a pair of B-spline curves running along the entire upper and lower mandible borders as auxiliary baselines, which provide a convenient reference framework for interpolation of curve cross-section surfaces, to extract the crucial geometry data of the original models from CT as NURBS contours. The distribution and curvature of the curve cross-section surfaces as well as the subdivision of the NURBS contours are well managed to allow a tight local mesh density control. The cortical layer and cancellous layer of the mandible mesh are constructed separately. And the quality of resulting FE mesh is quite satisfactory. In addition, the mesh structure properly accounts for the preferential direction dictated by the configuration of the mandible as well as the anisotropic material characteristics. With the help of the curve cross-section surfaces, the anisotropic FE model of the complete mandible is successfully generated by a well-established material assignment scheme.

7. Future plans

Taken together, although the anisotropic mandible FE model has to be validated in further studies, it seems that the developed modular software tool can provide an important component for developing a stand-alone computer-aided dental clinical plan software in the future, thus brings us one important step closer toward realizing the potential of FE modeling as an analytical tool in the investigation of clinical questions.

Further work involves addressing those problems discussed in Section 5.2. Furthermore, we focus on the studies of regional differences and to approach questions relating bone function of bone adaptation and growth, which rely on the information on the orientation of material axes, as well as those studies requiring the complete range of mandible, such as bending and torsion.

Acknowledgement

The research is supported by National Basic Research Program of China 2006CB303106.

REFERENCES

[1] R.T. Hart, V.V. Hennebel, N. Thongpreda, W.C. Buskirk, R.C. Anderson, Modeling the biomechanics of the mandible: a three-dimensional finite element study, J. Biomech. 25 (1992) 261–286.
[2] T.W. Korioth, A.G. Hannam, Deformation of the human mandible during simulated tooth clenching, J. Dent. Res. 73 (1994) 56–66.
[3] M.S. Shephard, M.K. Georges, Three-dimensional mesh generation by finite octree technique, Int. J. Numer. Methods Eng. 32 (1991) 709–749.
[4] J.R. Shewchuk, Tetrahedral mesh generation by Delaunay refinement, in: Proceedings of the Symposium on Computational Geometry, pp. 86–95 (New York, NY, 1998).
[5] R. Lohner, Progress in grid generation via the advancing front technique, Eng. Comput. 12 (1996) 186–210.
[6] S.H. Lo, Volume discretization into tetrahedral. II. 3D triangulation by advancing front approach, Comput. Struct. 39 (1991) 501–511.
[7] R. Schneiders, Grid-based algorithm for the generation of hexahedral element meshes, Eng. Comput. 12 (1996) 168–177.
[8] T.S. Li, R.M. McKeag, C.G. Armstrong, Hexahedral meshing using midpoint subdivision and integer programming, Comput. Methods Appl. Mech. Eng. 124 (1995) 171–193.
[9] T.D. Blacker, R.J. Myers, Seams and wedges in plastering: a 3D hexahedral mesh generation algorithm, Eng. Comput. 2 (1993) 89–93.
[10] T.J. Tautges, T. Blacker, S. Mitchell, The whisker-weaving algorithm: a connectivity based method for constructing all-hexahedral finite element meshes, Int. J. Numer. Methods Eng. 39 (1996) 3327–3349.
[11] S. Owen, A survey of unstructured mesh generation technology, in: Proceedings of the 7th International Meshing Roundtable, pp. 26–28 (Dearborn, Michigan, USA, 1998).

[12] S.-H. Teng, C.W. Wong, Unstructured mesh generation: theory, practice, perspectives, Int. J. Comput. Geom. Appl. 10 (2000) 227–266.
[13] M. Viceconti, C. Zannoni, L. Pierotti, Tri2solid: an application of reverse engineering methods to the creation of CAD models of bone segments, Comput. Methods Prog. Biomed. 56 (1998) 211–220.
[14] M. Viceconti, F. Taddei, Automatic generation of finite element meshes from computed tomography data, Crit. Rev. Biomed. Eng. 31 (2003) 27–72.
[15] C.L. Lin, H.E. Lee, C.H. Wang, K.H. Chang, Integration of CT, CAD system and finite element method to investigate interfacial stresses of resin-bonded prosthesis, Comput. Methods Prog. Biomed. 72 (2003) 55–64.
[16] R. Clement, J. Schneider, H.J. Brambs, A. Wunderlich, M. Geiger, F.G. Sander, Quasi-automatic 3D finite element model generation for individual single-rooted teeth and periodontal ligament, Comput. Methods Prog. Biomed. 73 (2004) 135–144.
[17] J.H. Keyak, J.M. Meagher, H.B. Skinner, C.D. Mote Jr., Automated three-dimensional finite element modelling of bone: a new method, J. Biomed. Eng. 12 (1990) 389–397.
[18] J.H. Keyak, S.A. Rossi, K.A. Jones, H.B. Skinner, Prediction of femoral fracture load using automated finite element modeling, J. Biomech. 31 (1998) 125–133.
[19] S.J. Hollister, B.A. Riemer, Digital image based finite element analysis for bone microstructure using conjugate gradient and Gaussian filter techniques, in: Proceedings of the Mathematical Methods in Medical Imaging II, SPIE Vol 2035, pp. 95–106 (San Diego, CA, USA, 1993).
[20] G.L. Niebur, M.J. Feldstein, et al., High-resolution finite element models with tissue strength asymmetry accurately predict failure of trabecular bone, J. Biomech. 33 (2000) 1575–1583.
[21] M. Viceconti, L. Bellingeri, L. Cristofolini, A. Toni, A comparative study on different methods of automatic mesh generation of human femurs, Med. Eng. Phys. 20 (1998) 1–10.
[22] D.L. Camacho, R.H. Hopper, G.M. Lin, B.S. Myers, An improved method for finite element mesh generation of geometrically complex structures with application to the skullbase, J. Biomech. 30 (1997) 1067–1070.
[23] Z.L. Wang, J.C. Teo, C.K. Chui, S.H. Ong, C.H. Yan, S.C. Wang, H.K. Wong, et al., Computational biomechanical modelling of the lumbar spine using marching-cubes surface smoothened finite element voxel meshing, Comput. Methods Prog. Biomed. 80 (2005) 25–35.
[24] J. Kaminsky, T. Rodt, A. Gharabaghi, J. Forster, G. Brand, M. Samii, A universal algorithm for an improved finite element mesh generation: mesh quality assessment in comparison to former automated mesh-generators and an analytic model, Med. Eng. Phys. 27 (2005) 383–394.
[25] C.L. Lin, C.H. Chang, C.S. Cheng, C.H. Wang, H.E. Lee, Automatic finite element mesh generation for maxillary second premolar, Comput. Methods Prog. Biomed. 59 (1999) 187–195.
[26] J. Gao, W. Xu, Z. Ding, 3D finite element mesh generation of complicated tooth model based on CT slices, Comput. Methods Prog. Biomed. 82 (2006) 97–105.
[27] N. Archip, R. Rohling, V. Dessenne, P.J. Erard, L.P. Nolte, Anatomical structure modeling from medical images, Comput. Methods Prog. Biomed. 82 (2006) 203–215.
[28] G.H. Kwon, S.W. Chae, K.J. Lee, Automatic generation of tetrahedral meshes from medical images, Comput. Struct. 81 (2003) 765–775.
[29] B. Erdmann, C. Kober, J. Lang, P. Deuflhard, H.-F. Zeilhofer, R. Sader, Efficient and Reliable Finite Element Methods for Simulation of the Human Mandible, in: Proceedings of the 9th Workshop on The Finite Element Method in Biomedical Engineering, Biomechanics and Related Fields, pp. 49–62 (Ulm, Germany, 2002).
[30] R. Taghavi, Automatic, parallel and fault-tolerant mesh generation from CAD, Eng. Comput. 12 (1996) 178–185.
[31] M. Viceconti, C. Zannoni, D. Testi, A. Cappello, A new method for the automatic mesh generation of bone segments from CT data, J. Med. Eng. Technol. 23 (1999) 77–81.
[32] M. Viceconti, M. Davinelli, F. Taddei, A. Cappello, Automatic generation of accurate subject-specific bone finite element models to be used in clinical studies, J. Biomech. 37 (2004) 1597–1605.
[33] C. Kober, M. Mülller-Hannemann, A case study in hexahedral mesh generation: simulation of the human mandible, Eng. Comput. 17 (2001) 249–260.
[34] V.B. Shim, R.P. Pitto, R.M. Streicher, P.J. Hunter, I.A. Anderson, The use of sparse ct datasets for auto-generating accurate FE models of the Femur and Pelvis, J. Biomech. 40 (2007) 26–35.
[35] Y. Zhang, C. Bajaj, B.S. Sohn, 3D finite element meshing from imaging data, Comput. Methods Appl. Mech. Eng. 194 (2005) 5083–5106.
[36] Y. Zhang, C. Bajaj, Adaptive, Quality quadrilateral/hexahedral meshing from volumetric data, Comput. Methods Appl. Mech. Eng. 195 (2006) 942–960.
[37] B. Couteau, Y. Payan, S. Lavallee, The mesh-matching algorithm: an automatic 3D mesh generator for finite element structures, J. Biomech. 33 (2000) 1005–1009.
[38] L. Baghdadi, D.A. Steinman, H.M. Ladak, Template-based finite-element mesh generation from medical images, Comput. Methods Prog. Biomed. 77 (2005) 11–21.
[39] S.C. Cowin (Ed.), Bone Mechanics Handbook, 2nd ed., CRC Press, Boca Raton, FL, 2001.
[40] J.Y. Rho, M.C. Hobatho, R.B. Ashman, Relations of mechanical properties to density and CT numbers in human bone, Med. Eng. Phys. 17 (1995) 347–355.
[41] D.C. Wirtz, N. Schiffers, T. Pandorf, K. Radermacher, D. Weichert, R. Forst, Critical evaluation of known bone material properties to realize anisotropic FE-simulation of the proximal femur, J. Biomech. 33 (2000) 1230–1325.
[42] F. Taddei, A. Pancanti, M. Viceconti, An improved method for the automatic mapping of computed tomography numbers onto finite element models, Med. Eng. Phys. 26 (2004) 61–69.
[43] R.B. Ashman, W.C. Van Buskirk, The elastic properties of a human mandible, Adv. Dent. Res. 1 (1987) 64–67.
[44] S. Lettry, B.B. Seedhom, E. Berry, M. Cuppone, Quality assessment of the cortical bone of the human mandible, Bone 32 (2003) 35–44.
[45] T. Nomura, E. Gold, M.P. Powers, S. Shingaki, J.L. Katz, Micromechanics/structure relationships in the human mandible, Dent. Mater. 19 (2003) 167–173.
[46] C.L. Schwartz-Dabney, P.C. Dechow, Edentulation alters material properties of cortical bone in the human mandible, J. Dent. Res. 81 (2002) 613–617.
[47] C.L. Schwartz-Dabney, P.C. Dechow, Variations in cortical material properties throughout the human dentate mandible, Am. J. Phys. Anthropol. 120 (2003) 252–277.
[48] A.M. O'Mahony, J.L. Williams, J.O. Katz, P. Spencer, Anisotropic elastic properties of cancellous bone from a human edentulous mandible, Clin. Oral Implants Res. 11 (2000) 415–421.
[49] M. Mülller-Hannemann, C. Kober, Anisotropic Validation of Hexahedral Meshes for Composite Materials in Biomechanics, in: Proceedings of the 10th International Meshing Roundtable, pp. 249–260 (Newport Beach, California, USA, 2001).
[50] A.M. O'Mahony, J.L. Williams, P. Spencer, Anisotropic elasticity of cortical and cancellous bone in the posterior mandible increases peri-implant stress and strain under oblique loading, Clin. Oral Implants Res. 12 (2001) 648–657.

[51] H.L. Huang, C.L. Lin, C.C. Ko, C.H. Chang, J.T. Hsu, J.S. Huang, Stress analysis of implant-supported partial prostheses in anisotropic mandibular bone: in-line versus offset placements of implants, J. Oral Rehabil. 33 (2006) 501–508.
[52] C. Montani, R. Scateni, R. Scopigno, Discretizied marching cubes, in: Proceedings of the IEEE Visualization '94' Congress, pp. 281–287 (Washington, DC, USA, 1994).
[53] J. Dompierre, P. Labbe, F. Guibault, R. Camarero, Proposal of Benchmarks for 3D Unstructured Tetrahedral Mesh Optimization, in: Proceedings of the 7th International Meshing Roundtable, pp. 459–478 (Dearborn, Michigan, USA, 1998).
[54] L. Peng, J. Bai, X. Zeng, Y. Zhou, Comparison of isotropic and orthotropic material property assignments on femoral finite element models under two loading conditions, Med. Eng. Phys. 28 (2006) 227–233.
[55] D.C. Wirtz, T. Pandorf, F. Portheine, K. Radermacher, N. Schiffers, A. Prescher, et al., Concept and development of an orthotropic fe model of the proximal femur, J. Biomech. 36 (2003) 289–293.